Rapid energy transfer in a dendrimer having π-conjugated light-harvesting antennas

I. Akai[1, 2], K. Miyanari[2], T. Shimamoto[1], A. Fujii[1], H. Nakao[3], A. Okada[3], K. Kanemoto[3], T. Karasawa[3], H. Hashimoto[3], A. Ishida[4], A. Yamada[4], I. Katayama[5], J. Takeda[4], M. Kimura[6]

[1] Shock Wave and Condensed Matter Research Center, Kumamoto University, 2-39-1 Kurokami, Kumamoto 860-8555, Japan

[2] Graduate School of Science and Technology, Kumamoto University, 2-39-1 Kurokami, Kumamoto 860-8555, Japan.

[3] CREST-JST & Department of Physics, Osaka City University, 3-3-138 Sugimoto, Sumiyoshi-ku, Osaka 558-8585, Japan.

[4] Department of Physics, Yokohama National University, 79-5 Tokiwadai, Hodogaya-ku, Yokohama 240-8501, Japan.

[5] Interdisciplinary Research Center, Yokohama National University, 79-5 Tokiwadai, Hodogaya-ku, Yokohama 240-8501, Japan.

[6] Department of Functional Polymer Science, Shinshu University, 3-15-1 Tokida, Ueda 386-8567, Japan.

E-mail: iakai@kumamoto-u.ac.jp

Abstract. We investigate rapid energy transfer (ET) and its temperature dependence in a star-shaped stilbenoid phthalocyanine (SSS1Pc) dendrimer having π-conjugated light-harvesting (LH) antennas, and develop an appropriate model. In SSS1Pc, an intense core photoluminescence (PL) band appears under the selective excitation of the absorption bands of the LH antenna due to highly efficient ET at room temperature. The transient response of core-absorption bleaching and the temporal behaviours of the PL intensities of the core and antenna reveal that ET from the LH antenna occurs rapidly prior to achieving quasi-equilibrium in the photoexcited state of the LH antenna. In addition, it is also clarified that the ET quantum efficiency in SSS1Pc degrades at temperatures lower than $\sim$100 K. To understand these results, we develop an ET model based on a π-conjugating network between the LH antenna and the core that accounts for steric hindrance between the LH antenna and the torsional vibration of the LH-antenna subunit. This model reveals that highly efficient ET occurs at room temperature through the π-conjugated network mediated by the thermally activated torsional vibration of the LH-antenna subunit.

PACS numbers: 33.50.-j, 33.50.Dq, 34.30.+h, 36.20.-r, 71.35.-y, 82.20.Rp

Submitted to: *New J. Phys.*

1. Introduction

Light-harvesting (LH) dendrimers [1, 2, 3, 4] have attracted considerable interest because they exhibit highly efficient energy transfer (ET) from LH antennas to cores [5]. The LH antennas in LH dendrimers have branching architectures consisting of π-conjugated aromatic rings and have high LH efficiencies in the visible and ultraviolet (UV) regions. Light energy absorbed by the LH antennas is transferred very efficiently to a central chromophore (core) [6, 7].

In large hyperbranched dendrimers, aromatic rings in the LH antenna are connected to each other by π-unconjugated spacer subunits such as ether subgroups ($-OCH_2-$). Owing to the isolation of the aromatic rings by these spacer subunits, the absorption bands of the LH antenna in such hyperbranched dendrimers appear in the ultraviolet region [5]. The ET processes in these dendrimers have been simplified to a Förster mechanism [8, 9, 10]. In the Förster mechanism [11], the ET donors and acceptors interact via the dipole-dipole interaction between the transition dipoles of the photoluminescence (PL) of the donors and the photoabsorption of the acceptors. This simplification of the ET mechanism is considered to be appropriate in these hyperbranched dendrimers because of the isolation of their aromatic rings. Recently, an advanced theoretical approach [12] has been developed for the ET process in LH dendrimers [13]. This approach involves calculating the exact Coulomb interactions between the electrons that contribute to ET. In addition, another group has proposed an improved Förster model, and they have applied the improved model to exciton migration phenomena in conjugated polymers [14, 15]. In this improved model, all of the electronic interactions promoting the ET process have been incorporated through the use of a multicentric monopole expansion in consideration of three-dimensional shape of the excited state wavefunctions. Furthermore, in this model, the spectral overlapping between the optical transitions of the ET donors and acceptors has been evaluated from quantitative computations of Franck-Condon factors both on high-frequency stretching and low-frequency ring-torsional modes. These sophisticated approaches on the ET processes have demonstrated the importance of microscopic and quantum-mechanical interaction to the ET process.

Another interesting aspect is the fact that the ET quantum efficiency β_{ET} is relatively high at room temperature (RT). In some kinds of dendrimers [5], β_{ET} at RT of greater than 80% have been reported. Although the core and the aromatic rings in LH antennas have rigid structures, the bonds connecting these rigid subgroups are highly flexible and can vibrate by changing their tilt and bending angles. At RT, such torsional and bending vibrations of adjoining bonds are expected to be activated since the frequencies of these vibrations are expected to be lower than the thermal energy at RT ($\sim$210 cm^{-1}) [16]. This suggests that such low-frequency vibrational modes play an important role in the highly efficient ET in LH dendrimers at RT.

In this paper, we investigate the ET process in a star-shaped stilbenoid phthalocyanine dendrimer (SSS1Pc) [17] that consists of oligo-phenylenevinylene

antennas and a phthalocyanine core. In SSS1Pc, the aromatic rings of the antenna are connected to the core by a π-conjugated vinylene subgroup. Consequently, SSS1Pc has a slightly planar structure due to the π conjugation between the core and oligo-phenylenevinylene antennas. In this dendrimer, the quantum efficiency of ET is evaluated from measurements of steady-state PL spectra obtained by selectively exciting the LH antenna. To understand the dynamics of ET, the temporal responses of the PL of the core and antennas and the ultrafast response of the transient absorption are measured under pulsed excitation of the LH antenna. In order to clarify the roles of the low-frequency vibrational modes in the ET process, we measure the temperature dependence of the PL spectra. In the discussion, we present a model for ET in SSS1Pc.

2. Experimental

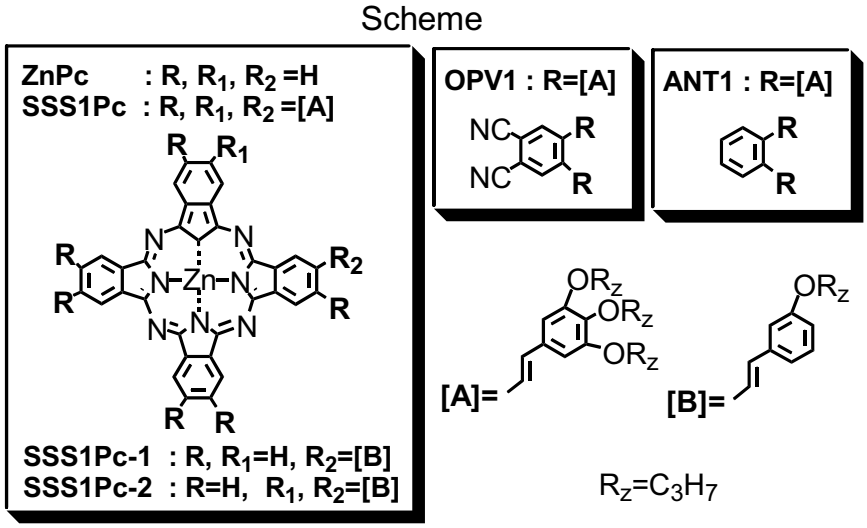

Figure 1. Chemical structures of SSS1Pc and its component molecules: ZnPc and OPV1. SSS1Pc-1, and -2 are model molecules given in [18]. ANT1 is a model molecule of a LH antenna subunit discussed in section 4.3.

The core and antenna subunits of SSS1Pc are zinc phthalocyanine (ZnPc) and oligo-phenylenevinylene (OPV1), respectively. The scheme shown in figure 1 indicates the chemical structures of SSS1Pc and its component molecules, ZnPc and OPV1. The crude products were purified by column chromatography and recycling preparative high precision liquid chromatography (HPLC) to obtain target molecules. The purity of target molecules were confirmed by analytical HPLC ($> 99\%$) and the isolated molecules were fully characterized by NMR and matrix-assisted laser-desorption ionization time-of-flight mass spectrometry. In the optical measurements, these molecules were diluted in anhydrous tetrahydrofuran (THF) to concentrations in the range $10^{-5} - 10^{-6}$ M.

Absorption spectra were recorded at RT using a Shimazu UV-2400 spectrophotometer with a spectral band width of 0.1 nm. The light output (2.95 eV) from a Xe lamp was used to measure the steady-state PL spectra of the dendrimer and its related

compounds. The spectral band width for detecting PL spectra is 0.2 nm (∼6 meV at Q-band PL). A double-grating monochromator (SPEX, model 270) was used to select the output light. The spectral band width of the excitation light was 0.04 eV at 2.95 eV. A solution of rhodamine 6G (Sigma-Aldrich) in ethanol was used as the standard for determining luminescence quantum yields. The excitation light intensity and the spectral sensitivity of the PL-detecting system were calibrated by using a standard tungsten lamp calibrated with NBS (No. EPT-1285) so that accurate measurements could be performed at different excitation photon energies.

In the time-resolved PL experiments, samples were excited with the second-harmonic output (∼3.1 eV) from a Ti:sapphire regenerative amplifier system (Spectra Physics, Hurricane-X). The pulse width of the excitation light was about 100 fs. The temporal responses of the PL intensities were recorded by a streak camera system (Hamamatsu Photonics, Model C2909) with a data-accumulation time of thirty minutes or one hour. The time resolution of the accumulated temporal responses of the PL intensity was approximately 20 ps as determined by a deconvolution analysis that used the exciting-laser profile obtained over the same accumulation time.

To measure the ultrafast ET dynamics in SSS1Pc, we employed a real-time pump-probe imaging spectroscopy method implemented on a single-shot basis. A Ti:sapphire regenerative amplifier system (Spectra Physics, Spitfire) with a pulse duration of ∼100 fs was used as the principal light source. The second-harmonic (3.1 eV) output of this laser system was used as the pump pulse. In the case of SSS1Pc, the intensity of the pump pulse is equivalent to an absorbed photon number density of 0.4 per dendrimer molecule. A probe pulse was generated by focusing the fundamental output of the laser system on a thin plate of CaF_2 . More details of this real-time pump-probe imaging spectroscopy method have been reported in previous papers [19, 20]. In order to avoid photodegradation and thermal heating of the samples [21], a solution of the samples was put in a 1-mm-thick disk-shaped quartz cell and the cell was rotated during the experiments. THF was used as the solvent and sample concentrations were in the range $10^{-4}-10^{-3}$ M. The temporal resolution of this experimental setup was about 130 fs [21].

In order to investigate the temperature dependence of ET, sealed quartz tubes filled with sample solutions in anhydrous THF were prepared. The freezing point of THF is about 165 K. A cryogenic refrigerator system (Nagase Electronic Equipment Service, model TS24SSR) was used for cooling and heating between RT and ∼4 K. In order to maintain the accuracy of temperature, the quartz tubes were mounted in a copper holder, which was attached tightly to the cooling stage of the cryogenic refrigerator. In addition, we waited for about one hour or longer to allow the temperature to stabilize before measuring each point. After each sequential measurement of the temperature dependence, we confirmed the reproducibility of the PL and absorption spectra at RT in order to verify that none of the samples had been damaged during cooling and heating.

The WinMOPAC package based on MOPAC97 [22] was used for quantum chemical calculations by using the PM3 Hamiltonian [23, 24].

3. Results

3.1. Absorption spectra

In SSS1Pc, the aromatic ring in the middle of the π-conjugated LH-antenna subgroup (OPV1) is shared with the phthalocyanine core as shown in figure 1. As a result of this sharing, the π-conjugated molecular orbitals (MOs) of the phthalocyanine core and the outer aromatic rings in the LH antenna are expected to be hybridised. This hybridisation may affect the absorption spectrum as well as ET.

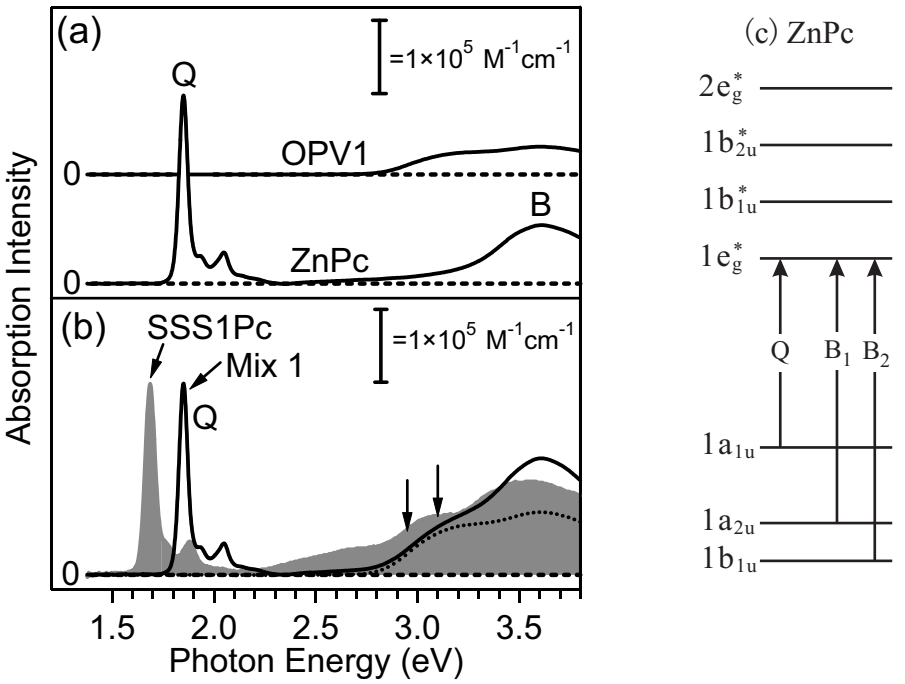

Figure 2. (a) absorption spectra of the component molecules ZnPc and OPV1. (b) absorption spectra of SSS1Pc (grey region) and Mix 1 (solid line) solutions. Arrows indicate the excitation energy for PL and pump-probe measurements. (c) Energy diagram of MOs for ZnPc (Fig. 8 in [25]) having D_{4h} symmetry. MOs lower than $1b_{1u}$ and MOs higher than $2e_g^*$ are omitted. Solid arrows indicate the optical transitions of the respective absorption bands (Q, Soret: B_1. B_2).

Figure 2-(a) shows absorption spectra of the component molecules ZnPc and OPV1. In the phthalocyanine ring of the core, optical transitions from the π-MOs to the first π*-MO give rise to the Q- and B-bands that are visible in the absorption spectrum of ZnPc (figure 2-(a)). An energy diagram for the π- and π*-MOs of ZnPc (Fig. 8 in [25]) is shown in figure 2-(c). The respective optical transitions (Q, B_1 and B_2) are indicated by the arrows in this figure. On the other hand, the absorption band due to the $\pi - \pi^*$ transition of the antenna-component molecule (OPV1) has a wide spectral width from 2.7 eV to higher energies reflecting the extended features of these MOs.

In order to compare with SSS1Pc, we also prepared mixture solutions containing the component molecules ZnPc and OPV1. The molar concentration ratio of OPV1 to

ZnPc was regulated so that the absorption spectrum of the mixture solutions gave a similar spectrum as SSS1Pc. Figure 2-(b) shows the absorption spectra of the SSS1Pc solution (grey region) and of the mixture solution Mix 1 (solid line) at RT. The molar concentration ratio of Mix 1 is 2.5. The dotted line indicates the enlarged absorption spectrum of OPV1 for this concentration ratio. The ratio agrees well with the expected ratio (2.7), which was derived by the following considerations. Since one of the three aromatic rings in OPV1 is shared with ZnPc, the eight units of the [A]-subgroup (see figure 1) in SSS1Pc correspond to the four molecules of OPV1 having two units (outer units) of the [A] subgroup. In this case, the molar concentration ratio should be ∼2.7 ($= 4 \times (2/3)$).

As figure 2-(b) shows, the Q-band in SSS1Pc appears at a lower energy than the Q-band in ZnPc. The origin of these Q-bands is a $\pi - \pi^*$ transition in an inner polyene ring composed of alternating π-conjugated bonding of carbon and nitrogen atoms in the phthalocyanine plane [25, 26]. The shift towards lower energies of the Q-band is considered to be due to the sharing of the aromatic ring in the π-conjugated antenna subgroups with the outer four benzo groups (see figure 1) in the phthalocyanine core. On the other hand, broad absorption bands at higher energies than the Q-band are ascribable to the sum of the $\pi - \pi^*$ transitions of the LH antenna and the B-band of the core. In the absorption spectrum of Mix 1, the lower energy tail region of the broad absorption band is found to be predominantly due to the $\pi - \pi^*$ transitions of the LH antenna, because the B-band of the core appears as a peak structure (3.6 eV) in the highest energy region of this broad absorption band. As indicated by the arrows (at 2.95 eV and 3.1 eV) in figure 2-(b), the exciting energy positions for the PL (section 3.2) and the pump-probe (section 3.4) experiments are located in the lower energy tail region of the broad absorption band in SSS1Pc. This confirms that the antenna subunits in SSS1Pc are predominantly excited by such selective excitation.

3.2. PL spectra

When the LH antennas are selectively excited, highly efficient ET occurs from the LH antenna to the core in SSS1Pc. Figure 3-(a) shows the PL spectra of SSS1Pc and Mix 1 solutions under such selective excitation. Since ET does not occur in Mix 1, there is an intense PL band due to the π^*-π transition in OPV1. The PL spectrum of SSS1Pc differs significantly from that of Mix 1. As shown in figure 3-(a), intense Q-band PL appears instead of the antenna PL in SSS1Pc. This transposition of the dominant PL is clear evidence for highly efficient ET from the LH antennas to the core in SSS1Pc. The highly efficient ET was confirmed by PL-excitation (PLE) measurements. The grey spectrum in figure 3-(b) is the PLE spectrum of the PL from the core in SSS1Pc. Since the PL intensity is proportional to the number of absorbed photons $A(E)$ and does not depend on the optical density (OD) of the absorption, the $A(E)$ spectrum was obtained by using the following conversion formula: $A(E) = 1 - 10^{-\mathrm{OD}}$. The $A(E)$ spectrum agrees well with the PLE spectrum as seen in figure 3-(b). This is conclusive evidence

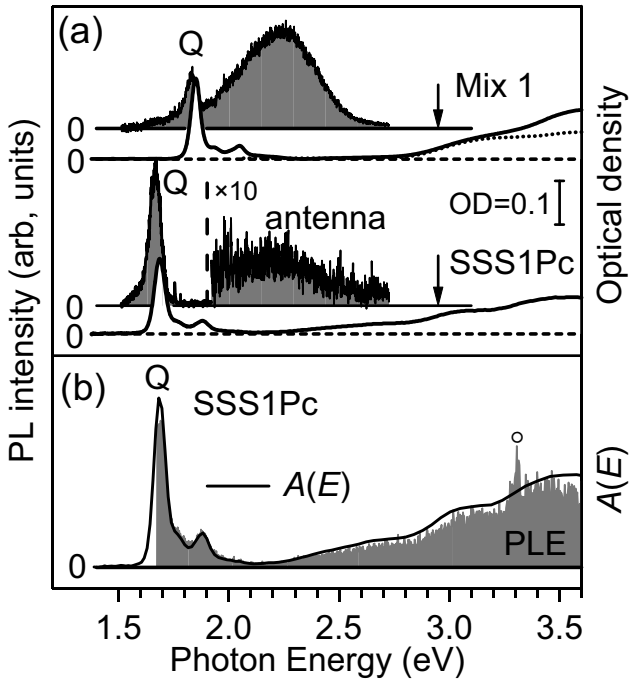

Figure 3. (a) PL spectra (grey region with solid line) of SSS1Pc and Mix 1 solutions. Absorption spectra denoted by OD are also indicated by solid lines. The PL intensities of SSS1Pc are enlarged by a factor of ten in the energy regions of the antenna-PL band. Arrows indicate the excitation energy. (b) PL excitation spectrum (grey region) for the core PL of SSS1Pc and absorbed photon-number spectrum $A(E)$. The peak structure (∘) at ∼3.4 eV is due to the second diffraction of the excitation light.

for highly efficient ET in SSS1Pc.

	E (eV)	Rhodamine 6G (R6G)	SSS1Pc	ZnPc
η^{X}	2.54	0.94 [27]		
	2.95	0.80±0.01	0.20±0.02	0.40±0.01
	1.96			0.3 [28]
β_{ET}	2.95		0.51±0.05 [29]	

Table 1. Luminescence quantum efficiency η and ET quantum efficiency β_{ET} at RT. A correction for the refractive indices of the solvents ($n_{\mathrm{ethanol}} = 1.3611$, $n_{\mathrm{THF}} = 1.4050$, [30]) has been performed, because the detection solid angles change depending on the refractive index of the solvent [31].

To quantitatively evaluate the ET quantum efficiency β_{ET} of SSS1Pc, the total luminescence quantum yields η^{X} (X = SSS1Pc, ZnPc) were measured by comparing with the PL intensity of a standard material, Rhodamine 6G (R6G). By using $\eta^{\mathrm{X}}(E)$, the PL intensity of the core PL $I^{\mathrm{X}}_{\mathrm{core}}(E)$ (Q-band) under photoexcitation with a photon energy E can be expressed as follows:

$$I^{\mathrm{X}}_{\mathrm{core}}(E) = \eta^{\mathrm{X}}(E)\, A^{\mathrm{X}}(E), \quad (\mathrm{X} = \mathrm{SSS1Pc}, \mathrm{ZnPc}) \tag{1}$$

where $A^{\mathrm{X}}(E)$ is the number of absorbed photons ($A(E) = 1 - 10^{-\mathrm{OD}}$) at E. Since η^{X} depends on E, the luminescence quantum yield $\eta^{\mathrm{R6G}}(2.95\ \mathrm{eV})$ for excitation at 2.95 eV was obtained by using a reference value of $\eta^{\mathrm{R6G}}(2.54\ \mathrm{eV})$ (see table 1) [27]; the values thus obtained are listed in table 1. From these values, $\eta^{\mathrm{SSS1Pc}}(2.95\ \mathrm{eV})$ and $\eta^{\mathrm{ZnPc}}(2.95\ \mathrm{eV})$ were obtained as shown in table 1. Since the value obtained for $\eta^{\mathrm{ZnPc}}(2.95\ \mathrm{eV})$ is approximately consistent with the previously reported value [28], it is considered that these values are sufficiently accurate for evaluating the ET quantum efficiency.

In SSS1Pc, since PL of the core is observed after ET, η^{SSS1Pc} can be written as a product of η^{ZnPc} and the ET quantum efficiency β_{ET}, as follows:

$$\eta^{\mathrm{SSS1Pc}} = \beta_{\mathrm{ET}}\, \eta^{\mathrm{ZnPc}}. \tag{2}$$

From this equation, β_{ET} was evaluated to be 0.51 at RT by using the values in table 1. This result implies that the ET from the LH antennas is efficient in SSS1Pc.

In the following section, we describe the temporal behaviours of the PL intensities for understanding the dynamics of this highly efficient ET.

3.3. Temporal behaviour of PL

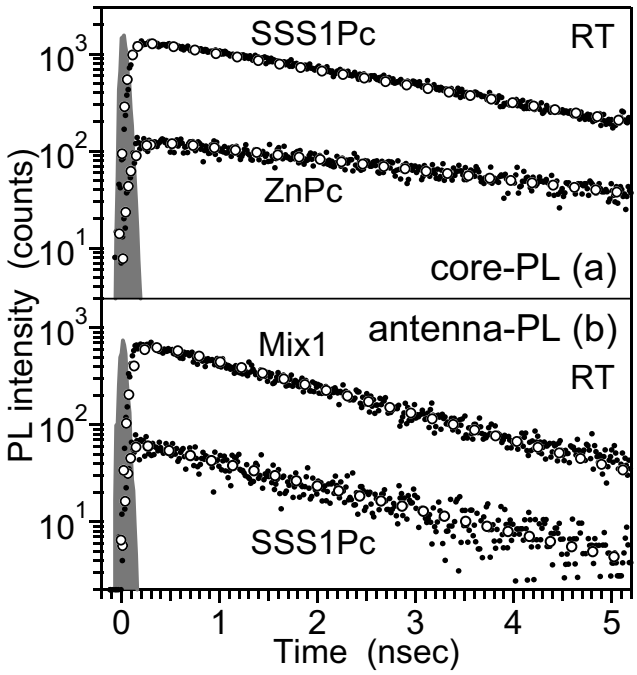

Figure 4. Decay profiles of PL intensities (a) of the core and (b) of the antenna (filled dots). Grey profiles are the measured temporal profiles of the excitation light pulse. Profiles indicated by open circles are the fitting results of deconvolution analysis.

Figure 4 shows the temporal responses of the PL intensities for (a) the core in SSS1Pc and ZnPc and (b) the antennas in SSS1Pc and Mix 1. In this figure, experimental results are represented by filled dots. Grey profiles at $t \sim 0$ are the temporal profiles of the excitation laser pulse measured using the streak camera

SSS1Pc		ZnPc	Mix 1
Core	Antenna	Core	Antenna
$\tau_{\mathrm{Core}}^{\mathrm{SSS1Pc}}$ (ns)	$\tau_{\mathrm{Ant}}^{\mathrm{SSS1Pc}}$ (ns)	$\tau_{\mathrm{Core}}^{\mathrm{ZnPc}}$ (ns)	$\tau_{\mathrm{Ant}}^{\mathrm{OPV1}}$ (ns)
2.3 ± 0.2	1.5 ± 0.2	3.7 ± 0.3	1.6 ± 0.2

Table 2. Decay time constants of the PL intensities for the core and antennas obtained by deconvolution analysis. The error margins for the decay time constants are the uncertainty widths obtained by deconvolution analysis.

system. By using these profiles, the decay time constants of the respective decay profiles were obtained by deconvolution analysis by assuming only one single-exponential decay component; these decay time constants are listed in table 2. Fitted results are represented by open circles in figure 4, and reproduce well the experimental results.

Two important points should be noted regarding these results. The first is that the decay time constant $\tau_{\mathrm{Ant}}^{\mathrm{SSS1Pc}}$ (that for the PL of the antennas in SSS1Pc) is rather long in spite of the highly efficient ET from the LH antennas in SSS1Pc. This value is almost the same as that for the component molecule of the antennas, OPV1 ($\tau_{\mathrm{Ant}}^{\mathrm{OPV1}}$), lying within the uncertainties of the deconvolution analysis.

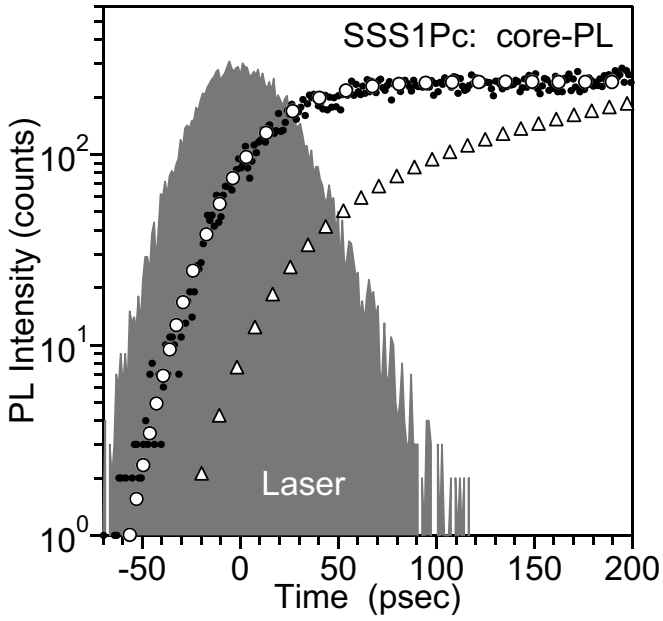

Figure 5. Rising behaviour of the PL for the core in SSS1Pc (filled dots). Grey profiles are observed temporal profiles of the excitation light pulses. Profiles indicated by open circles and triangles are simulation results using values for the rising time constant τ_{rise} of 0.02 ns and 1.5 ns ($\tau_{\mathrm{Ant}}(\mathrm{RT})$), respectively.

The second point to note from the results is the rapid rising time of the PL intensity of the core in SSS1Pc. To verify this, we measured the rising behaviour with a high temporal resolution. The dotted plots in figure 5 indicate the results for SSS1Pc with selective excitation of the LH antenna absorption band ($E = 3.1$ eV). The grey profile

denotes the temporal profile of the excitation pulse; the observed pulse has a full width at half maximum (FWHM) of about 50 ps. The open triangles show the simulation result obtained by deconvolution analysis by assuming that the rising time constant for the energy acceptor state (core) is equivalent to the decay time constant ($\tau_{\mathrm{Ant}}^{\mathrm{SSS1Pc}} = 1.5$ ns in table 2) of the energy donor state (LH antenna). However, the PL intensity for the core in SSS1Pc rises more rapidly than this simulation result, as figure 5 shows. A clear rising component cannot be resolved in the deconvolution analysis for this rapid rising behaviour because of the limited time resolution ($\sim$ 20 ps). Open circles represent the simulation results obtained by deconvolution analysis without a rising component.

These two points give clear experimental evidence for rapid ET in SSS1Pc. If the luminescent state in the antennas were an energy donor state for ET to the core, a clear delaying behaviour having the same time constant as the decay of the energy donor state should be observed in the increase in the PL intensity of the core. In SSS1Pc, however, the rising of the PL of the core is much faster than the decay time constant of the PL of the antennas. This result clearly implies that ET occurs prior to thermal equilibrium of the photoexcited state being achieved in the LH antenna.

3.4. Ultrafast transient absorption

In order to clarify the ultrafast dynamics of the rapid ET in SSS1Pc, we applied a real-time pump-probe imaging spectroscopy to SSS1Pc. The grey spectra in figure 6 are time-resolved absorbance change spectra obtained 3 ps after selective excitation of the LH-antenna absorption band ($E = 3.1$ eV; arrows in figure 6, pulse width $\sim$100 fs in FWHM). The dark-grey and light-grey areas indicate bleaching of the absorption and induced absorption by pumping, respectively. The ordinary absorption spectra without pumping are also displayed by dashed lines. In OPV1 shown in figure 6-(c), a positive transient absorption band appears over the entire energy region. This induced absorption can be assigned to an optical transition from the excited states to higher excited states. Bleaching of the Q-band absorption (1.7$\sim$2.0 eV) and an induced absorption band in the high-energy region ($>$ 2.0 eV) are visible in the spectrum for ZnPc (figure 6-(b)). The Q-band bleaching is obvious and it is plotted on a scale that is a factor of 10 smaller than the rest of the spectrum. Obvious bleaching of the Q-band can also been seen in the SSS1Pc spectrum shown in figure 6-(a). In the case of SSS1Pc, the induced absorption above $\sim$2.0 eV is considered to be due to the induced absorption bands of both the core and the antenna subunits.

For times longer than 3 ps but shorter than 10 ps, there is no evident decay, because the excited state that cause spectral changes has decay time constants that are of the order of nanoseconds (see table 2). However, a different rising behaviour is clearly evident in the transient responses of the Q-band bleachings in SSS1Pc and ZnPc. The dark-grey regions in figure 7 indicate the ultrafast responses of Q-band bleaching in (a) ZnPc and (b) SSS1Pc. In the case of ZnPc, Q-band bleaching commences immediately after the pumping pulse (dotted line). For a time constant of a single exponential rise

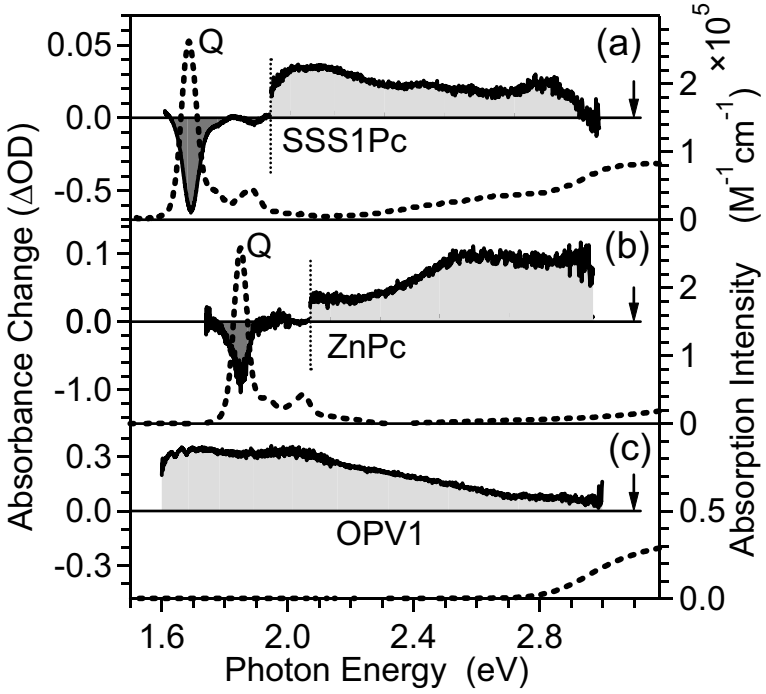

Figure 6. Transient absorption change spectra for (a) SSS1Pc, (b) ZnPc, and (c) OPV1. Grey spectra indicate transient absorption change spectra at 3 ps (2.5∼3.5 ps) after photoexcitation. Dashed lines show the normal absorption spectra without pumping. Dark and light grey areas denote bleaching of absorption and induced absorption, respectively. The arrows indicate the energy of the pump laser. The increments of the vertical scale are increased by a factor of 10 in the vicinity of the Q-band.

for Q-band bleaching in ZnPc, an ultrashort time constant of ∼100 fs was obtained by deconvolution analysis. Fitted results are indicated by open circles in figure 7-(a). This ultrafast rising indicates that the photoexcited state relaxes to the lowest-lying Q-band state within ∼100 fs. By contrast, Q-band bleaching in SSS1Pc increases more slowly as shown in figure 7-(b), in which the rising behaviour of ZnPc is also plotted for reference. From deconvolution analysis, the rising time constant of SSS1Pc $\tau_{\mathrm{ET}}^{\mathrm{SSS1Pc}}$ is estimated to be ∼250 fs. The fitted results (open circles in figure 7-(b)) accurately reproduces the experimental results.

3.5. Temperature dependence

The internal molecular vibrations of the aromatic rings inside the LH antenna of dendrimers in which the LH antennas have a branching architecture are highly flexible. Although the aromatic rings have a rigid structure, these aromatic rings are connected to each other by adjoining subgroups and can vibrate at the adjoining subgroup. In dendrimers having benzyl ethyl-ether LH antenna [32, 33], in which ethyl-ether subgroups make up the adjoining subunit, we have reported that the quantum efficiency of the ET from the LH antenna to the core increases with heating from 4 K to ∼100 K

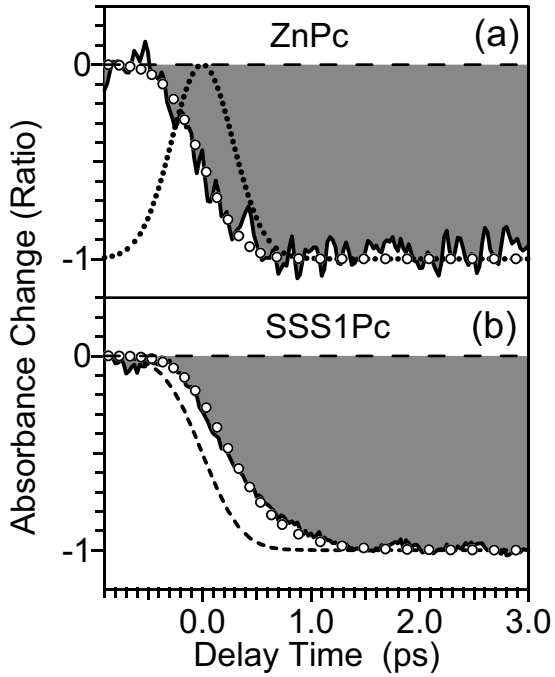

Figure 7. Ultrafast responses of bleaching of the Q-absorption band for (a) ZnPc and(b) SSS1Pc. The dotted line in (a) indicates the temporal profile of the instrument response function. Dark-grey regions indicate the temporal profiles of the Q-band bleachings. Fitted results with respective rising components are plotted using open circles. The dashed line in (b) is a visual guide and indicates the fitted result for ZnPc (open circles in (a)).

[34]. This result clearly shows that molecular vibrations with frequencies less than $\sim$70 cm^{-1} (= k_BT; T =100 K) play an important rule in the highly efficient ET in these dendrimers. In these dendrimers, torsional and bending vibrations at the ethyl-ether subunits are considered to be important [34], because they are expected to have frequencies lower than 70 cm^{-1} [35, 36, 37]. In this section, we present the experimental results for the temperature dependence of the PL spectra and the decay time constants of SSS1Pc. The temperature dependence of the quantum efficiency of the ET and a physical insight into the temperature dependence will be discussed in section 4.2 and 4.3.

The temperature dependences of the PL spectra were measured in the temperature range from 4 K to RT under selective excitation of the antenna-absorption bands (2.95 eV). In Mix 1, an intense PL band of the antennas due to OPV1 appears at RT as shown in figure 3-(a). Although the PL intensities of ZnPc and OPV1 change with temperature, the dominance of PL of OPV1 in Mix 1 does not change over the entire temperature range (4 K$\sim$RT). Figure 8-(a) shows the temperature dependence of the ZnPc-PL spectrum in Mix 1. The PL intensity due to ZnPc increases slightly on cooling from RT (297 K) to 180 K. The PL intensity decreases once at 140 K on further cooling beyond the freezing point (FP)(160 K) of the solvent (THF). The solutions

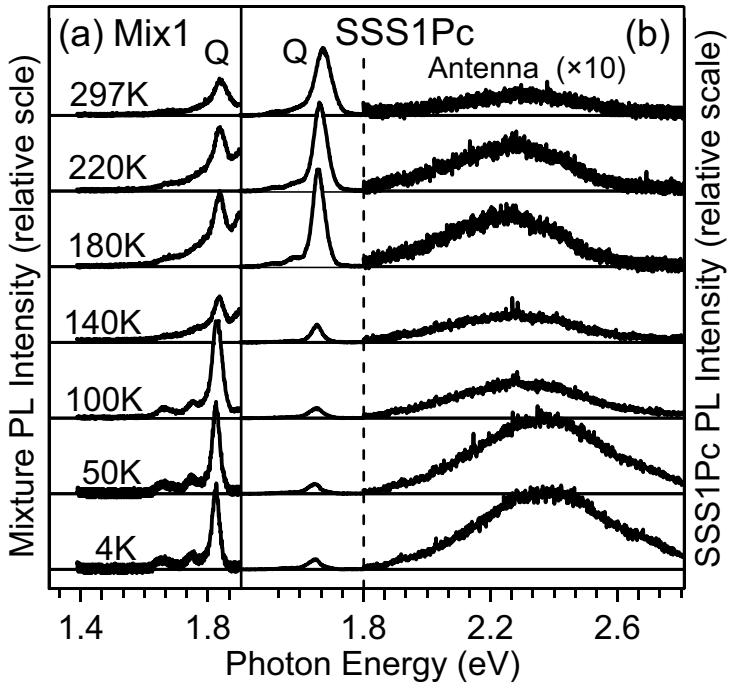

Figure 8. Temperature dependence of the PL spectra of (a) SSS1Pc and the PL of the core in Mix 1 (b). The PL intensities for the antennas in SSS1Pc are enlarged by a factor of ten.

become cloudy at temperatures below the freezing point, due to the solvent freezing. The suppression in the PL intensity at 140 K is considered to be due to the cloudiness of the solution. This situation does not change below 100 K. However, the PL of the core (ZnPc) in Mix 1 becomes intense, overcoming the cloudiness of the solution (see figure 8-(a)). In contrast, the PL spectrum of SSS1Pc changes drastically with temperature as shown in figure 8-(b). At temperatures above the FP, the highly efficient ET gives rise to an intense PL band from the core, as can be seen in the PL spectra at 297 $\sim$ 180 K in figure 8-(b), where the PL intensities of the antenna are plotted on a scale that is enlarged by a factor of ten. At 140 K, the intensities of both PL bands decrease once in analogy with Mix 1. However, on cooling below the FP, the PL intensities of the core and antenna exhibit quite different dependences, as can be seen in figure 8-(b). The PL intensity of the core decreases slightly from 100 K to 4 K. On the other hand, the PL intensity of the antenna becomes intense. This result suggests that the ET in SSS1Pc quenches below 100 K.

Figure 9-(a) shows the temperature dependence of the PL intensities of the core $I_{\rm Core}$ (filled circles) and of the antenna $I_{\rm Ant}$ (open circles) in SSS1Pc, in which the ordinate is normalized for the entire PL at $T = 297$ K and the vertical broken line indicates the FP temperature of the solvent (THF). The suppression of the $I_{\rm Core}$ below 100 K suggests that the quantum efficiency $\beta_{\rm ET}$ of the ET in SSS1Pc decreases considerably below 100 K. Since the PL intensities $I_{\rm Core}$ and $I_{\rm Ant}$ depend on $\beta_{\rm ET}$ as well as the quantum yields of the PL of the core and the antennas, we also evaluated the decay

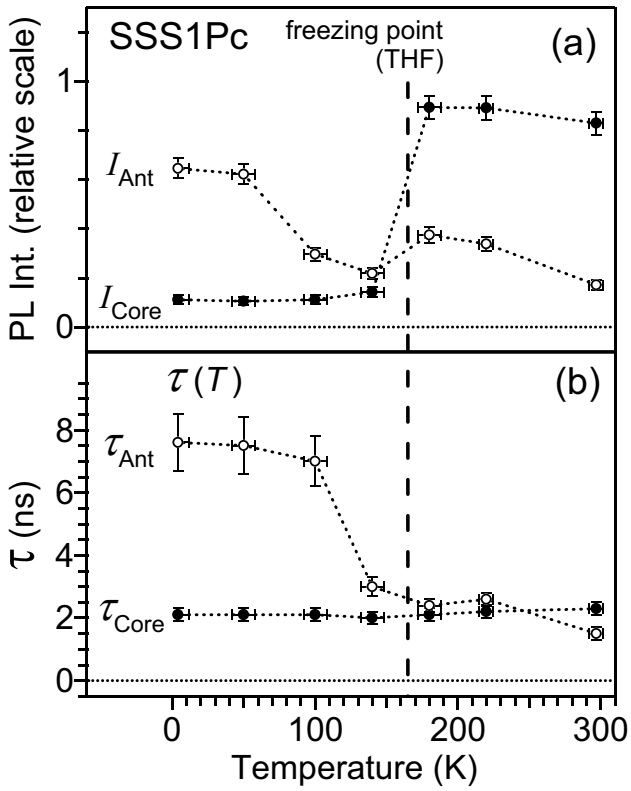

Figure 9. (a) Temperature dependence of the PL intensities of the core I_{Core} (•) and of the antennas I_{Ant} (○). (b) Temperature dependence of the decay time constants for the PL of the core τ_{Core} (•) and for the PL of the antennas τ_{Ant} (○). The vertical broken line indicates the freezing point of the solvent THF. The magnitude of the error bar indicate the error width of 1σ.

time constants τ_{Core} and τ_{Ant} of the PL intensities of the core and antennas in order to quantitatively determine the temperature dependence of β_{ET}. Figure 9-(b) shows the temperature dependence of these decay time constants. In section 4.2, the temperature dependence of the ET quantum efficiency β_{ET} is discussed in terms of our ET model.

4. Discussion

In the previous section, experimental results were presented for ET in SSS1Pc dendrimers. Three key points of these results are summarized as follows: (1) an intense PL band of the core appears under the selective excitation of the antenna-absorption band owing to the highly efficient ET. (2) ET occurs rapidly with a faster rising time constant than the decay time constant of the PL of the antennas. (3) At temperatures below ∼100 K, the PL of the core in SSS1Pc is greatly suppressed, suggesting that ET is partially inhibited below ∼100 K. In the following sections, we address some key issues for gaining a deeper understanding of the ET processes in SSS1Pc, and describe a model for the ET process in SSS1Pc.

4.1. Energy transfer process

As mentioned in section 1, in the case of large hyperbranched dendrimers, the Förster mechanism has been used to describe ET from the relaxed luminescent states of the antennas to the core [8, 9, 10]. This is because the aromatic rings in the LH antennas are connected to each other by π-unconjugated spacer subgroups. Owing to these spacer subgroups, the π- and π*-MOs of these aromatic rings in the LH antennas do not overlap with each other beyond the spacer subgroups. In the case of the Förster mechanism [11], the decay time constant of the PL of the antennas τ_{Ant} is shorter than when ET does not occur. This is due to the interactions between the transition dipoles of PL of the antennas and core absorption. Furthermore, the PL intensity of the core exhibits a delayed rising behaviour with the same time constant τ_{Ant} [8, 9]. These things are clear evidence for highly efficient ET by the Förster mechanism. However, as demonstrated in section 3.3 and 3.4, such evidence cannot be resolved in SSS1Pc. The decay time constant of the PL of the antennas $\tau_{\mathrm{Ant}}^{\mathrm{SSS1Pc}}$ in SSS1Pc (1.5 ± 0.2 ns) is almost the same as $\tau_{\mathrm{Ant}}^{\mathrm{OPV1}}$ (1.6 ± 0.2 ns) in Mix 1 (see table 2). Furthermore, the rising time constant $\tau_{\mathrm{ET}}^{\mathrm{SSS1Pc}}$ ($\sim$ 250 fs) of the Q-band absorption bleaching (figure 7) is much faster than $\tau_{\mathrm{Ant}}^{\mathrm{SSS1Pc}}$. These facts clearly indicate that the rapid ET in SSS1Pc cannot be explained by the Förster mechanism.

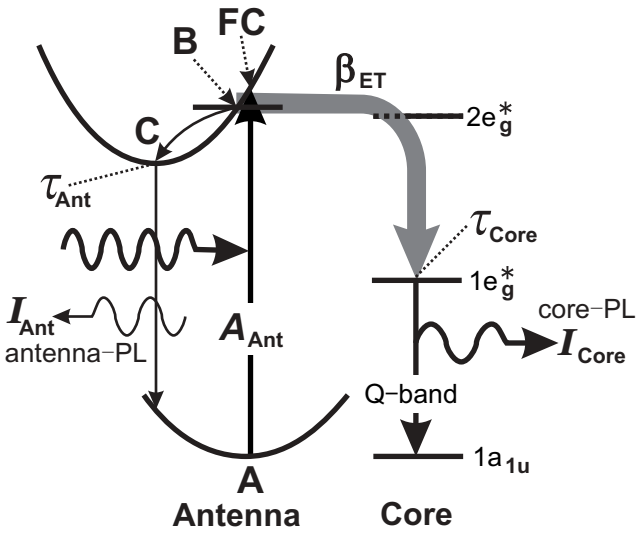

Figure 10. A simple model for the rapid ET in SSS1Pc under selective excitation of the LH antennas.

To understand this rapid ET in SSS1Pc, we consider the energy diagram shown in figure 10. As figure 3 shows, the PL of the antennas (2.0∼2.6 eV) in SSS1Pc (and also in Mix 1) appears with a large Stokes shift (> 0.5 eV). This means that the PL of the antennas occurs after deep vibrational relaxations in the LH antennas. Therefore, in our simple model shown in figure 10, we take into account the vibrational relaxation from the Franck-Condon (FC) state (point FC in figure 10) to the luminescent state

(point C) of the LH antennas. The model also takes the $2e_g^*$ state (see figure 2-(c)) in the phthalocyanine core into consideration. Since the $2e_g^*$ state is located at an energy that is ∼1.7 eV higher than the $1e_g^*$ state [25, 38], the $2e_g^*$ state (∼ 3.6 eV above $1a_{1u}^*$) is expected to be located at approximately the resonant energy position of the FC state of the LH antennas (see figure 10). Furthermore, the $2e_g^*$ state contains a major portion of the MO of the outer benzo groups of the phthalocyanine core [25], which are shared with the LH-antenna subunits. On the other hand, the π^*-MO of the LH-antenna subunit (phenylenevinylene) extends considerably along the phenylenevinylene chain. Based on the morphology of the $2e_g^*$ MO in the core and the π^* MO in the LH antennas, these MOs are expected to interact with each other.

For an ET mechanism that involves short-range interactions, one can consider the Dexter ET mechanism [39, 40]. In this mechanism, an electron exchange interaction is responsible for the ET from the energy donor to the energy acceptor via the overlapping of their wavefunctions. In SSS1Pc, since the aromatic ring in the middle of the phenylenevinylene chain in the LH antennas is shared with the phthalocyanine core (see figure 1), there is considered to be sufficient overlapping of the wavefunctions for the Dexter ET mechanism. However, a recent theoretical investigation [18] found an energy transfer process through a π-conjugated network by using a time-dependent density functional theory. In this investigation, Y. Kodama *et al.* simulated the one-way ET from the LH antennas to the core in the model molecules of SSS1Pc, and discovered that wave packets of excited electrons and holes in the LH antennas propagate to the core extremely rapidly (∼10 fs) in a completely planar model molecule SSS1Pc-1 (see figure 1), which has only one [B]-subgroup (≈[A]-subgroup in SSS1Pc) [18]. This simulation result clearly demonstrates that the rapid ET in SSS1Pc is due to the ultrafast propagation of the excited electrons and holes from the LH antennas to the core via the π-conjugated network that exists between them.

In addition to such direct interactions through the π-conjugated network, one should consider vibrational motion of each subunit and vibrational relaxation of the excited state in the ET donor. In the improved Förster model by E. Hennebicq *et al.* [14], they have distinguished the ET processes to two limiting cases depending on the relative magnitude of the electronic interactions responsible for the ET process, V_{DA}, and the vibrational relaxation energy of the excited state in the ET donor, $E^{\mathrm{D}}_{\mathrm{relax.}}$. The "original" Förster mechanism [11] is the weak regime of V_{DA}, in which the ET takes place subsequently to the vibrational relaxation in the ET donor [14]. On the other hand, in the strong interaction limit ($V_{\mathrm{DA}} \gg E^{\mathrm{D}}_{\mathrm{relax.}}$), the excitation wave packet in the ET donor spread over the whole system without any self-localization by the vibrational relaxation [14]. In SSS1Pc, the ET process can be classified into such strong interaction cases, because the π^* MO of the LH antennas (donor) and the $2e_g^*$ MO of the core (antenna) are overlapped each other sufficiently at the outer benzo groups of the phthalocyanine core.

4.2. Temperature dependence of $\beta_{\rm ET}$

In section 3.5, the PL intensities and the decay time constants of the PL of the core and antennas in SSS1Pc were found to change drastically with temperature (see figure 8 and 9). In this section, we clarify the temperature dependence of the ET quantum efficiency $\beta_{\rm ET}$ by applying a simple model (figure 10) to our experimental results.

In this model, we neglect the direct excitation of the core since the LH antennas in SSS1Pc are selectively excited as described in section 3.1. We consider the rapid ET from the ET donor state (B state in figure 10) near the FC state in the LH antennas (see figure 10). By assuming that the quantum yield of the relaxation from the FC state to the donor state is unity, the number of donor states is given by the number of photons absorbed by the LH antennas $A_{\rm Ant}$ $(= 1 - 10^{-{\rm OD}_{\rm Ant}})$. In this model, the PL intensities $I_{\rm Core}$ and $I_{\rm Ant}$ can be described as follows:

$$I_{\rm Core} = A_{\rm Ant}\,\beta_{\rm ET}\,\frac{\tau_{\rm Core}}{\tau_{\rm Core}^{\rm rad.}}, \qquad I_{\rm Ant} = A_{\rm Ant}\,(1-\beta_{\rm ET})\,\gamma_{\rm Ant}\,\frac{\tau_{\rm Ant}}{\tau_{\rm Ant}^{\rm rad.}}, \tag{3}$$

where $\tau_{\rm Core}$ and $\tau_{\rm Ant}$ denote the decay time constants of the luminescent states of the core ($1e_g^*$ in figure 10) and the LH antennas (C in figure 10) respectively, and $\tau_{\rm Core}^{\rm rad.}$ and $\tau_{\rm Ant}^{\rm rad.}$ are the radiative lifetimes of the respective luminescent states. Also, $\gamma_{\rm Ant}$ represents the quantum yield of the vibrational relaxation from the donor state to the luminescent state inside the LH antenna. From equation (3), the ET quantum efficiency $\beta_{\rm ET}(T)$ is derived as

$$\beta_{\rm ET}(T) = \left(1 + \frac{1}{\Gamma}\,\frac{\tau_{\rm Core}(T)}{\tau_{\rm Ant}(T)}\,\frac{I_{\rm Ant}(T)}{I_{\rm Core}(T)}\right)^{-1}, \qquad \frac{1}{\Gamma} \equiv \frac{1}{\gamma_{\rm Ant}}\,\frac{\tau_{\rm Ant}^{\rm rad}}{\tau_{\rm Core}^{\rm rad}}. \tag{4}$$

In section 3.2, $\beta_{\rm ET}({\rm RT})$ was calculated to be 0.51 from the luminescence quantum yields of SSS1Pc and ZnPc (table 1). From this value of $\beta_{\rm ET}({\rm RT})$ and the values of $\tau_{\rm Core}$, $\tau_{\rm Ant}$, $I_{\rm Core}$ and $I_{\rm Ant}$ (table 2 and figure 3), and by assuming that the quantum yield of the relaxation from the $2e_g^*$ state to the $1e_g^*$ state is unity, the value of Γ is calculated to be $\sim$0.33.

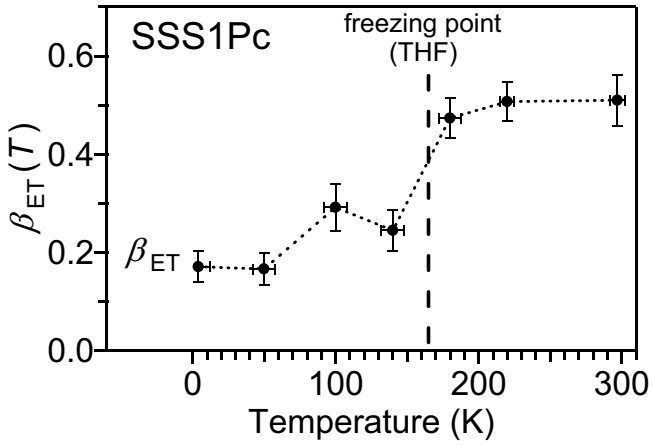

Figure 11. Filled circles: temperature dependence of the ET quantum efficiency $\beta_{\rm ET}$ in SSS1Pc. The vertical broken line indicates the FP of the solvent (THF).

By using equation (4) and the experimental results in figure 9, the temperature dependence of $\beta_{\rm ET}$ can be found by assuming that the parameters in Γ (equation (4)) are unaffected by thermal perturbations. In figure 11, $\beta_{\rm ET}$ are plotted as a function of temperature. The vertical error bars indicate the uncertainty (1σ) of $\beta_{\rm ET}$ and are obtained from the error bars for the decay time constants and the PL intensities. As figure 11 clearly shows, $\beta_{\rm ET}(T)$ has a remarkable temperature dependence. At temperatures higher than 140 K, $\beta_{\rm ET}(T)$ remains almost constant, having approximately the same value as that at RT (=0.51). On cooling, $\beta_{\rm ET}(T)$ decreases considerably and is ~ 0.17 at 4 K. This result clearly demonstrates that the rapid ET in SSS1Pc degrades at temperatures lower than ~ 100 K, and suggests that the freezing of molecular vibrations at low temperatures greatly affects rapid ET in SSS1Pc.

4.3. Temperature dependence of energy transfer

As discussed in section 4.1, the π-conjugated network between the LH antennas and the core is responsible for the highly efficient and rapid ET in SSS1Pc. To form this π-conjugated network, a high coplanarity between the planes of the LH antennas and the phthalocyanine core is essential. However, coplanarity is inhibited by steric hindrance and molecular vibrations in the LH-antenna subunits of SSS1Pc. In fact, Y. Kodama *et al.* have clarified that the one-way transfer of electrons and holes is strongly suppressed in a model molecule SSS1Pc-2 (see figure 1) that has two [B]-subgroups. The coplanarity in SSS1Pc-2 is worse than that in SSS1Pc-1 because the LH-antenna subunits ([B]-subgroups) are tilted at the vinylene joint due to the steric hindrance between the terminal subgroups $-{\rm OR_z}$ (see figure 1). In addition, torsional vibrations are expected to alter the tilting angle Θ between the planes of the core and the [A]-subgroup (see figure 1) and they are activated at RT. In this section, we qualitatively discuss the effect of steric hindrance and torsional vibration pf the LH antennas on the temperature dependence of the rapid ET.

To discuss the steric hindrance and the temperature dependence of the torsional vibrations in the LH antennas, we employ a simple model molecule for the LH antenna subunit (ANT1) in figure 1 and analyse it using the WinMOPAC software. Figure 12-(a) shows an optimised structure of ANT1 for the ground state. As can be seen in this figure, due to the steric hindrance between the terminal subgroups ($-{\rm OR_z}$), the aromatic rings in the LH antennas are tilted relative to the plane of the aromatic ring in the phthalocyanine core. Such degradation of the coplanarity between the aromatic rings of the LH antennas and the phthalocyanine core is expected to suppress the rapid ET process mediated by the π-conjugation network. However, by considering the torsional vibration of the aromatic rings in the LH antennas, we can gain a qualitative understanding the temperature dependence of the ET process in SSS1Pc. A normal coordinate analysis of the optimised structure reveals that the torsional vibration of the aromatic rings in the LH antennas ([A] in figure 1) is the lowest normal vibration mode with a frequency of ~ 8 cm^{-1}, which agrees well with that (8 cm^{-1}) for *trans*-stilbene

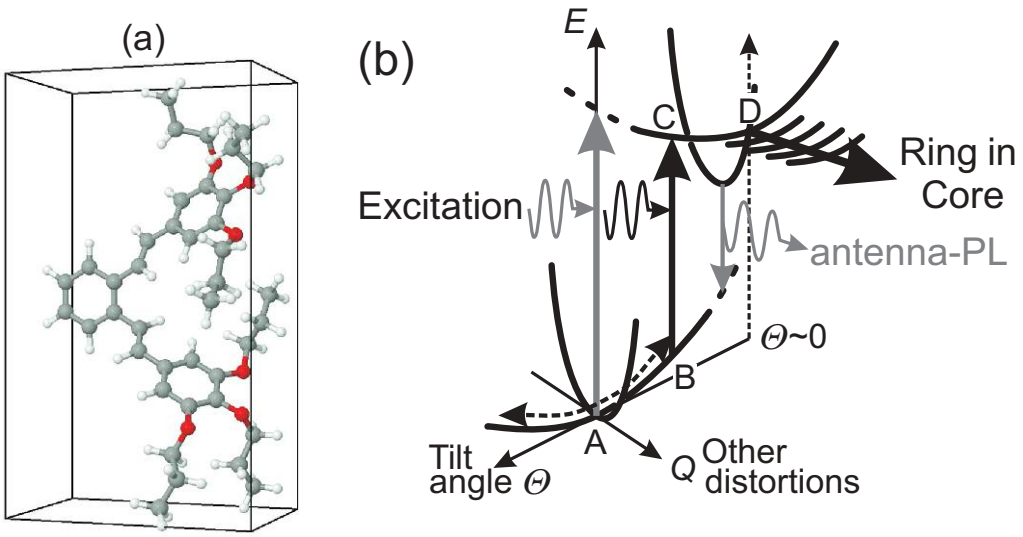

Figure 12. (a) Optimised structure of the model molecule ANT1 in figure 1. (b) Schematic diagram of the adiabatic potentials of the ground and excited states considering the torsional vibration (tilt angle Θ) and other normal-mode vibrations (Q).

reported in [41]. In this mode, the aromatic rings in the LH antennas vibrate at the vinylene joint, changing the tilt angle Θ relative to the plane of the aromatic ring in the phthalocyanine core. At higher temperatures, the coplanarity between the aromatic ring in the LH antennas and the core changes dynamically due to the thermal activation of this torsional vibration. To understand the temperature dependence of ET in SSS1Pc, we employ a simplified model that accounts for this torsional vibration.

Figure 12-(b) shows a schematic diagram of the adiabatic potentials in the ground and excited states of the LH-antenna subunit. In this diagram, two coordinates are introduced for describing the adiabatic potentials. The first is the tilt angle Θ between the aromatic rings in the LH antennas and the core. The curvature of the adiabatic potential as a function of Θ is gentle, reflecting the low frequency of the torsional vibration (~ 8 cm^{-1}). The second coordinate is the configuration coordinate Q, which represents all the other normal coordinates that vibrate with high frequencies. In the ground state, a potential minimum (point A in figure 12-(b)) is located at a large tilt angle Θ due to the steric hindrance between the antenna subunits. However, the potential minimum is expected to be different in the excited state (based on π^* MOs). The quasi-equilibrium point on Θ for the excited state is thought to be located near $\Theta \sim 0$ (point D in figure 12-(b)) [16], because in the excited state the bond alternation at the vinylene joint is partially released due to the extension of the π^* MOs [16]. As a result of the relaxation along Θ on the adiabatic potential, a planar structure ($\Theta \sim 0$, D in figure 12-(b)) is more feasible in the excited state. Such a planar structure is anticipated to give rise to highly efficient ET via the π-conjugated network [18], as indicated by the thick solid arrow in figure 12-(b).

By considering the thermal behaviour in the adiabatic potential of the ground

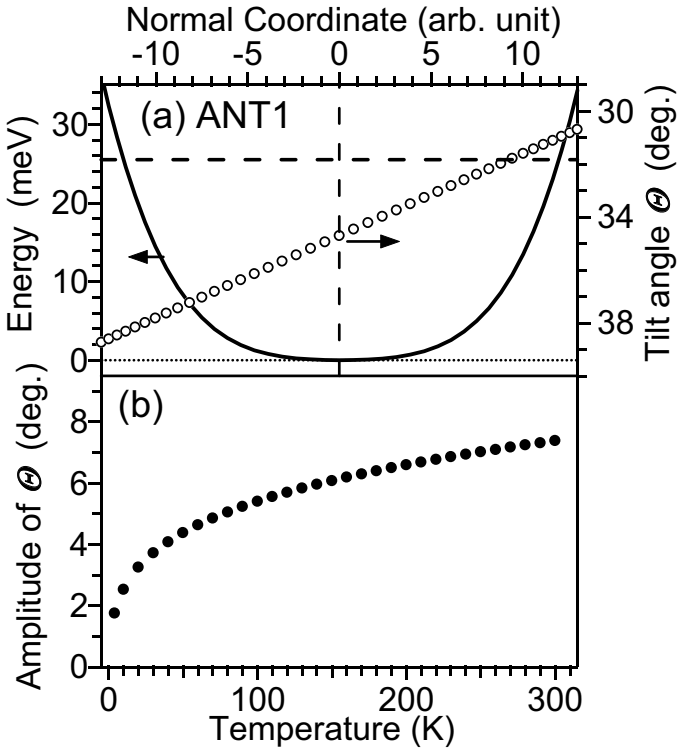

Figure 13. (a) Adiabatic potential (solid line) and tilt angle Θ (open circles) as functions of the normal coordinate. (b) Temperature dependence of the amplitude of Θ.

state, we can qualitatively understand the temperature dependence of the ET quantum efficiency $\beta_{\rm ET}$ in SSS1Pc. The solid line in figure 13-(a) shows the adiabatic potential of the torsional vibration (the lowest mode: 8 $\rm cm^{-1}$) obtained through calculations of the self-consistent field energies of respective vibrating structures. The horizontal broken line represents the thermal energy at RT. Θ is plotted with open circles in figure 13-(a) as a function of the normal coordinate. At a low temperature $\sim$ 0 K, Θ fluctuates about the equilibrium position with a small amplitude. In this case, the coplanarity between the aromatic rings in the LH antennas and the phthalocyanine core is not so good because of the tilting of the aromatic rings in the LH antenna due to steric hindrance, and selective excitation of the LH antennas is only available from point A in figure 12-(b). The FC state just above point A is far from the point where $\Theta \sim 0$ (point D). On the other hand, the amplitude of Θ increases at higher temperatures, as shown by the open circles in figure 13-(b), and the probability of higher coplanarity (smaller Θ) increases with the torsional vibration. Thus, excitation from points with a smaller Θ (point B in figure 12-(b)) is enabled at higher temperatures. After the excitation from point B, the FC state (point C in figure 12-(b)) relaxes toward the intermediate bottom with $\Theta \sim 0$ (point D), and the excited state can propagate along the ET channel due to the effective connection with the core provided by the π-conjugated network. It is expected that during the relaxation along Θ, relaxation due to other distortions toward

the bottom of the adiabatic potentials also occurs. However, at higher temperatures, since it is possible to excite the FC state near $\Theta \sim 0$, ET is expected to occur prior to other distortions. Consequently, the ET quantum efficiency β_{ET} is expected to improve at higher temperatures, as shown in figure 11.

5. Conclusion

We have investigated the ET process in the SSS1Pc dendrimer having π-conjugated LH antennas and have developed a simple model for the ET process.

In SSS1Pc, an intense PL band for the core appears under the selective excitation of the antennas due to the highly efficient ET from the antennas to the core. From the comparison of the temporal behaviours of PL intensities of the core and antennas and the transient absorption spectra under the selective excitation of the antenna, it is found that a rapid ET occurs from the antennas prior to thermal equilibrium being achieved for the photoexcited state in the LH antennas. On the basis of the temperature dependences of the core and antenna PL intensities and their decay time constants in SSS1Pc, the temperature dependence of the ET quantum efficiency β_{ET} is evaluated quantitatively, and it is demonstrated that the rapid ET in SSS1Pc is strongly suppressed by further cooling below ∼100 K.

To explain both the rapid rising behaviour and the temperature dependence of ET, we developed a model that accounts for the steric hindrance between the LH-antenna subunits and the torsional vibration of the aromatic rings in the LH antennas. On the basis of the thermal behaviour of the torsional vibration in the ground state, it is concluded that the highly efficient ET at RT is realized via the π-conjugated network mediated by the thermally activated torsional vibration.

References

[1] A. Adronov and J. M. J. Fréchet. Light-harvesting dendrimers. *Chem. Commun.*, pages 1701–1710, 2000.

[2] D. A. Tomalia, H. Baker, J. Dewald, M. Hall, G. Kallos, S. Martin, J. Roeck, J. Ryder, and P. Smith. A new class of polymers: Starburst-dendritic macromolecules. *Polym. J.*, **17**:117–132, 1985.

[3] S. M. Grayson and J. M. J. Fréchet. Convergent dendrons and dendrimers: from synthesis to applications. *Chem. Rev.*, **101**:3819–3867, 2001.

[4] D. A. Tomalia, A. M. Naylor, and W. A. Goddard III. Starbust dendrimers: Molecular-level control of size, shape, surface chemistry, topology, and flexibility from atoms to macroscopic matter. *Angew. Chem. Int. Ed.*, **29**:138–175, 2003.

[5] D.-L. Jiang and T. Aida. Morphology-dependent photochemical events in aryl ether dendrimer porphyrins: Cooperation of dendron subunits for singlet energy transduction. *J. Am. Chem. Soc.*, **120**:10895–10901, 1998.

[6] C. Devadoss, P. Bharathi, and J. S. Moore. Energy transfer in dendritic macromolecules: Molecular size effects and the role of an energy gradient. *J. Am. Chem. Soc.*, **118**:9635–9644, 1996.

[7] D. Liu, S. De Feyter, M. Cotlet, A. Stefan, U.-M. Wiesler, A. Herrmann, D. Grebel-Koehler, J. Qu, K. Müllen, and F. C. De Schryver. Fluorescence and intramolecular energy transfer in polyphenylene dendrimers. *Macromol.*, **36**:5918–5925, 2003.

[8] M.-S. Choi, T. Aida, T. Yamazaki, and I. Yamazaki. Dendritic multiporphyrin arrays as light-harvesting antennae: Effects of generation number and morphology on intramolecular energy transfer. *Chem. Eur. J.*, **8**:2668–2678, 2002.

[9] P. R. Hania, D. J. Heijs, T. Bowden, A. Pugžlys, J. van Esch, J. Knoester, and K. Duppen. Ultrafast energy transport in a first-generation coumarin-tetraphenylporphyrin dendrimer. *J. Phys. Chem. B*, **108**:71–81, 2004.

[10] I. Akai, T. Kato, K. Kanemoto, T. Karasawa, M. Ohashi, S. Shinoda, , and H. Tsukube. Morphology dependence of excitonic energy transfer in light-harvesting dendrimers having benzyl ether-type peripheries. *phys. stat. sol. (c)*, **3**:3420–3425, 2006.

[11] T. Förster. 10th spiers memorial lecture - transfer mechanisms of electronic excitation. *Discuss. Faraday Soc.*, **27**:7–17, 1959.

[12] B. P. Krueger, G. D. Scholes, and G. R. Fleming. Calculation of couplings and energy-transfer pathways between the pigments of lh2 by the ab initio transition density cube method. *J. Phys. Chem. B*, **102**:5378–5386, 1998.

[13] W. Ortiz, B. P. Krueger, V. D. Kleiman, J. L. Krause, and A. E. Roitberg. Energy transfer in the nanostar: The role of coulombic coupling and dynamics. *J. Phys. Chem. B*, **109**:11512–11519, 2005.

[14] E. Hennebicq, G. Pourtois, G D. Scholes, L. M. Herz, D. M. Russell, C. Silva, S. Setayesh, A. C. Grimsdale, K. Müllen, J.-L. Brédas, and D. Beljonne. Exciton migration in rigid-rod conjugated polymers: An improved förster model. *J. Am. Chem. Soc.*, **127**:4744–4762, 2005.

[15] H. Wiesenhofer, D. Belijonne, G. D. Scholes, E. Hennebicq, J.-L. Brédas, and E.Zojer. Limitations of the förster description of singlet exciton migration: The illustrative example of energy transfer to ketonic defects in ladder-type poly(*para*-phenylense). *Adv. Funct. Mater.*, **15**:155–160, 2005.

[16] S. Karabunarliev, M. Baumgarten, and K. Müllen. Adiabatic one- and two-photon excited states in phenylene-based conjugated oligomers: A quantum-chemical study. *J. Phys. Chem. A*, **104**:8236–8243, 2000.

[17] M. Kimura, H. Narikawa, K. Ohta, K. Hanabusa, H. Shirai, and N. Kobayashi. Star-shaped stilbenoid phthalocyanines. *Chem. Mater.*, **14**:2711–2717, 2002.

[18] Y. Kodama, S. Ishii, and K. Ohno. Dynamics simulation of a π-conjugated light-harvesting dendrimer. *J. Phys.: Condens. Matter*, **19**:365242, 2007.

[19] N. Furukawa, C. E. Mair, V. D. Kleiman, and J. Takeda. Femtosecond real-time pump.probe imaging spectroscopy. *Appl. Phys. Lett.*, **85**:4645–4647, 2004.

[20] Y. Makishima, N. Furukawa, A. Ishida, and J. Takeda. Femtosecond real-time pump-probe imaging spectroscopy implemented on a single shot basis. *Jpn. J. Appl. Phys.*, **45**:5986–5989, 2006.

[21] A. Ishida, Y. Makishima, A. Okada, I. Akai, K. Kanemoto, T. Karasawa, M. Kimura, and J. Takeda. Time.frequency two-dimensional mapping of rapid energy transfer in light-harvesting star-shaped dendrimers. *J. Lumin.*, **128**:771–773, 2008.

[22] J. J. P. Stewart. *MOPAC97 Manual*. Fujitsu Limited, 1997.

[23] J. J. P. Stewart. Optimization of parameters for semiempirical methods i. method. *J. Comp. Chem.*, **10**:209–220, 1989.

[24] J. J. P. Stewart. Optimization of parameters for semiempirical methods ii. applications. *J. Comp. Chem.*, **10**:221–264, 1989.

[25] S. P. Keizer, J. Mack, B. A. Bench, S. M. Gorun, and M. J. Stillman. Spectroscopy and electronic structure of electron deficient zinc phthalocyanines. *J. Am. Chem. Soc.*, **125**:7067–7085, 2003.

[26] M. J. Stillman and T. Nyokong. *Phthalocyanines: Properties and Applications*, chapter 3 Absorption and Magnetic Circular Dichroism Spectral Properties of Phthalocyanines Part 1, pages 133–287. John Wiley & Sons Inc, 1989.

[27] M. Fischer and J. Georges. Fluorescence quantum yield of rhodamine 6g in ethanol as a function of concentration using thermal lens spectrometry. *Chem. Phys. Lett.*, **260**:115–118, 1996.

[28] P. S. Vincett, E. M. Voigt, and K. E. Rieckhoff. Phosphorescence and fluorescence of phthalocyanines. *J. Chem. Phys.*, **55**:4131–4140, 1971.

[29] I. Akai, A. Okada, K. Kanemoto, T. Karasawa, H. Hashimoto, and M. Kimura. Quenching of energy transfer by freezing molecular vibrations in light-harvesting small dendrimer. *J. Lumin.*, **119-120**:283–287, 2006.

[30] H. P. R. Frederikse and D. R. Lide, editors. *CRC Handbook of Chemistry and Physics*. CRC-Press, 1978.

[31] J. R. Lakowicz. *Principles of Fluorescence Spectroscopy 2nd Ed.*, chapter 2.10 Quantum yield standards, pages 52–53. Plenum Pub Corp, 1999.

[32] D.-L. Jiang and T. Aida. *Dendrimers and Other Dendritic Polymers*, chapter 17 Dendritic Polymers: Optical and Photochemical Properties, pages 425–439. John Wiley & Sons Inc, 2001.

[33] S. Shinoda, M. Ohashi, and H. Tsukube. "pocket dendrirners" as nanoscale receptors for bimolecular guest accommodation. *Chem. Eur J.*, **13**:81–89, 2007.

[34] I. Akai, T. Kato, A. Okada, K. Kanemoto, T. Karasawa1, M. Kimura, M. Ohashi, S. Shinoda, and H. Tsukube. Depression of excitonic energy transfer by freezing molecular vibrations in meta-linked branching dendrimers. *phys. stat. sol. (c)*, **3**:3414–3419, 2006.

[35] S. Hamatani, K. Tsuji, A. Kawai, and K. Shibuya. Dispersed fluorescence spectra of jet-cooled benzophenone ketyl radical: Assignment of the low-frequency vibrational modes. *Phys. Chem. Chem. Phys.*, **5**:1370–1375, 2003.

[36] R. L. de Sousa, J. L. A. Alves, and H. W. Leite Alves. Vibrational properties of ppp and ppv. *Mater. Sci. Eng. C*, **24**:601–605, 2004.

[37] M. Tsuge, S. Hamatani, A. Kawai, K. Tsuji, and K. Shibuya. Jet spectroscopy of arylmethyl radicals in the visible region: assignment of low-frequency vibrational modes in diphenylmethyl and chlorodiphenylmethyl radicals. *Phys. Chem. Chem. Phys.*, **8**:256–263, 2006.

[38] J. Mack and M. J. Stillman. Band deconvolution analysis of the absorption and magnetic circular dichroism spectral data of znpc(-2) recorded at cryogenic temperatures. *J. Phys. Chem.*, **9**:7935–7945, 1995.

[39] D. L. Dexter. A theory of sensitized luminescence in solids. *J. Chem. Phys.*, **21**:836, 1953.

[40] V. Bulović, M. A. Baldo, and S. R. Forrest. *Organic Electronic Materials / Conjugated Polymers and Low molecular Weight Organic Solids*, chapter 11.2.4 Electronic Energy Transfer, pages 401–404. Springer, 2001.

[41] T. Suzuki, N. Mikami, and M. Ito. Two-color stimulated emission spectroscopy of trans-stilbene: Large amplitude torsional motion in the ground state and its role in intramolecular vibrational redistribution. *J. Phys. Chem.*, **90**:6431–6440, 1986.